NUMERICAL AND STATISTICAL ANALYSES OF A NATURAL CONVECTION RADIATIVE HYBRID NANOFLUID FLOW ON A VERTICAL PERMEABLE PLATE

Nur Syahirah WAHID[1,*], Mohd Shafie MUSTAFA[1], Norihan MD ARIFIN[1,2], Najiyah Safwa KHASHI'IE[3], Ioan POP[4,5]

[*1]Department of Mathematics and Statistics, Faculty of Science Universiti Putra Malaysia, 43400 UPM Serdang, Selangor, Malaysia

[2]Institute for Mathematical Research, Universiti Putra Malaysia, 43400 UPM Serdang, Selangor, Malaysia

[3]Fakulti Teknologi dan Kejuruteraan Mekanikal, Universiti Teknikal Malaysia Melaka, Hang Tuah Jaya, 76100 Durian Tunggal, Melaka, Malaysia

[4]Department of Mathematics, Babeş-Bolyai University, R-400084 Cluj-Napoca, Romania

[5]Academy of Romanian Scientists, 3 Ilfov Street, 050044 Bucharest, Romania

[*]Corresponding author; syahirahwahid@upm.edu.my

This study presents the mathematical and statistical findings towards the model of steady, laminar, natural convection hybrid alumina-copper/water nanofluid flow on a vertical permeable hot plate with a thermal radiation effect. The governing partial differential equations of the model are simplified to a system of ordinary differential equations by using the sophisticated similarity transformation. For mathematical analysis, a finite difference method is used via the numerical solver known as bvp4c (Matlab) while for statistical analysis, a response surface methodology (RSM) is adapted via Minitab. It is found that the stronger thermal radiation effect improves the heat transmission rate of the hybrid nanofluid under the presence of suction and natural convection. This finding has been statistically proven through the optimization technique via RSM with 99.97% desirability.

Key words*: Hybrid nanofluid, suction, thermal radiation, vertical plate, response surface methodology*

1. Introduction

The well-established fluid known as nanofluid has achieved significant success in many technical applications especially in fields involving heat transmission, including electronics cooling, engines, and refrigeration systems, as well as in biomedical applications such as targeted drug delivery and diagnostic imaging. This fluid was first proposed by Choi and Eastman [1] to improve the performance of the working fluid. Nanofluid is created by suspending an adequate concentration of nanoparticles in an industrial base fluid. Even though nanofluid is assisting researchers in their pursuit of thermal efficiency, scientists are still looking for an improved kind of working fluid. To address these issues, a more advanced category of nanofluid called hybrid nanofluid has been developed. A hybrid nanofluid is created by spreading diverse types of nanoparticles as independent components or by scattering nanocomposite particles in the base fluid [2]. Similar to conventional nanofluid, the goal of adopting hybrid nanofluid is to further enhance the heat transmission and pressure drop properties

by balancing the benefits and drawbacks of separate suspensions, which are ascribed to a better thermal network, aspect ratio, and synergistic impact of nanomaterials [3].

Several experimental investigations also have proven the thermal capability of hybrid nanofluid such as those that have been conducted by Suresh et al. [4, 5]. According to their studies, the hybridization of metallic copper nanoparticles with alumina nanoparticles results in a considerable improvement in heat transmission performance. This has captivated our attention to also consider alumina and copper in our present boundary layer flow study. In the context of numerical findings, especially for the case of boundary layer flow, Devi and Devi [6] conducted a numerical investigation on the flow of hybrid copper-alumina nanofluid past a stretched sheet. Their results stated that it is possible to obtain an ideal heat transmission rate of a hybrid nanofluid, which is by selecting different quantities of nanoparticles that are appropriate for the conditions. They then extended the study towards the three-dimensional configuration with Newtonian heating. In this study too, their findings have proven that hybrid nanofluid performs better than the convectional nanofluid [7]. Ever since these earlier studies, a large number of researchers, including Wahid et al. [8], Mohd et al. [9], Khashi'ie et al. [10], Yahaya et al. [11], Algehyne et al. [12], and others, have been focusing their attention on hybrid nanofluid by taking into account a variety of different physical assumptions for the fluid flow model in order to solve the real phenomena of application.

Therefore, in this study, we aim to explore the natural convective flow of a hybrid nanofluid on a vertical permeable plate with the existence of thermal radiation. This present study is also an advancement from the previous study performed by Zeyghami and Rahman [13]. We have improved their study by considering the hybrid nanofluid model with the adoption of thermophysical correlations by Takabi and Salehi [14]. We also inserted the thermal radiation parameter by using the Rosseland approximation, while considering a permeable plate surface with suction. Both numerical and statistical approaches are used to simulate the present flow model. Hence, this study could provide significant insight from both numerical and statistical perspectives regarding the heat transmission performance of hybrid nanofluid.

2. Mathematical formulation

We take into consideration the two-dimensional, steady, laminar, boundary layer flow of hybrid nanofluid over a vertical permeable hot plate, which is driven by the buoyancy forces as depicted in Fig. 1, where x - axis is measured in the vertical direction which is parallel to gravitational acceleration g, and y - axis is normal to the surface of the plate, while the flow being in the region $y \geq 0$. It is assumed that the velocities along (x, y) axes are (u, v). The mass flux velocity is v_w such that $v_w < 0$ is for suction and $v_w > 0$ is for injection. T, T_w and T_∞ are the temperature of the hybrid nanofluid, constant plate temperature and ambient temperature, respectively. Radiative heat flux q_r with no scattering effect is considered. The viscous dissipation has been disregarded in the energy equation, due to the small velocities associated with the free stream convection. Hybrid nanoparticles (i.e., alumina and copper) are dispersed into water for the formation of hybrid nanofluid. The correlations and the values for the hybrid nanofluid thermophysical

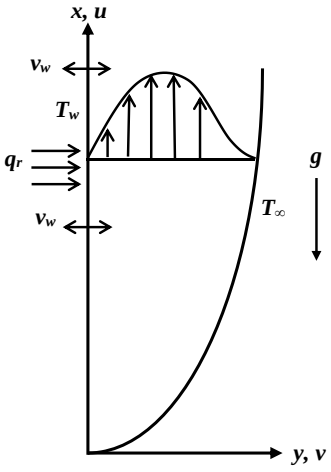

Figure 1. Physical model illustration

properties are followed from those given by Takabi and Salehi [14], and Oztop and Abu-Nada [15] (see Tabs. 1 and 2).

Table 1. Correlations of the thermophysical properties

Properties	Correlations
Density	$\rho_{hnf} = \rho_{s1}\phi_1 + \rho_{s2}\phi_2 + \rho_f(1-\phi_{hnf})$ where $\phi_{hnf} = \phi_1 + \phi_2$
Heat Capacity	$\left(\rho C_p\right)_{hnf} = (\rho C_p)_{s1}\phi_1 + (\rho C_p)_{s2}\phi_2 + (\rho C_p)_f\left(1-\phi_{hnf}\right)$
Dynamic Viscosity	$\mu_{hnf} = \mu_f\left(1-\phi_{hnf}\right)^{-2.5}$
Thermal Conductivity	$k_{hnf} = \left[\dfrac{2k_f + \left(\dfrac{\phi_1 k_{s1} + \phi_2 k_{s2}}{\phi_{hnf}}\right) + 2\left(\phi_1 k_{s1} + \phi_2 k_{s2}\right) - 2\phi_{hnf} k_f}{2k_f - \left(\phi_1 k_{s1} + \phi_2 k_{s2}\right) + \left(\dfrac{\phi_1 k_{s1} + \phi_2 k_{s2}}{\phi_{hnf}}\right) + \phi_{hnf} k_f}\right] \times k_f$
Thermal expansion	$\beta_{hnf} = \dfrac{1}{\rho_{hnf}}\left(\phi_1\rho_{s1}\beta_{s1} + \phi_2\rho_{s2}\beta_{s2} + \left(1-\phi_{hnf}\right)\rho_f\beta_f\right)$

Table 2. Thermophysical properties

Properties	Base fluid	Nanoparticles	
	Water (f)	Alumina $(s1)$	Copper $(s2)$
Density, $\rho\left(\mathrm{kg/m^3}\right)$	997.1	3970	8933
Specific Heat Capacity, $C_p\left(\mathrm{J/kgK}\right)$	4179	765	385
Electric conductivity, $k\left(\mathrm{W/mK}\right)$	0.613	40	400
Thermal expansion, $\beta\left(\mathrm{1/K}\right)$	21×10^{-5}	0.85×10^{-5}	1.67×10^{-5}
Prandtl number, Pr	6.2		

In these tables, ϕ is the volume fraction of the nanoparticles where ϕ_1 corresponds to alumina and ϕ_2 corresponds to copper. The fluid is reduced to regular fluid when $\phi_1 = \phi_2 = 0$. It should be noted that the subscript of *hnf, f, s1* and *s2* refer to hybrid nanofluid, base fluid, the first type of nanoparticles (alumina), and the second type of nanoparticles (copper), respectively.

Under the abovementioned assumptions, the governing equations for the model can be expressed as (see Zeyghami and Rahman [13]; Devi and Devi [16]):

$$\frac{\partial u}{\partial x} + \frac{\partial v}{\partial y} = 0, \tag{1}$$

$$u\frac{\partial u}{\partial x} + v\frac{\partial u}{\partial y} = \frac{\mu_{hnf}}{\rho_{hnf}}\frac{\partial^2 u}{\partial y^2} + \beta_{hnf}\left(T - T_\infty\right)g, \tag{2}$$

$$u\frac{\partial T}{\partial x} + v\frac{\partial T}{\partial y} = \frac{k_{hnf}}{\left(\rho C_p\right)_{hnf}}\frac{\partial^2 T}{\partial y^2} - \frac{1}{\left(\rho C_p\right)_{hnf}}\frac{\partial q_r}{\partial y}, \tag{3}$$

subject to the boundary conditions

$$\begin{aligned} &u = 0,\ v = v_w,\ T = T_w \text{ at } y = 0, \\ &u \to 0,\ T \to T_\infty \text{ as } y \to \infty. \end{aligned} \tag{4}$$

Following Rosseland approximation [17-19], the radiative heat flux q_r can be equated as follows:

$$q_r = -\frac{4\sigma^*}{3k^*}\frac{\partial T^4}{\partial y}, \tag{5}$$

where k^* and σ^* denote the coefficient of mean absorption and the constant of Stefan-Boltzmann, respectively. Adopting the Taylor series and neglecting the higher-order terms, T^4 is expanded about T_∞ to obtain $T^4 \approx 4T_\infty^3 T - 3T_\infty^4$ so that the energy equation can be equated as

$$u\frac{\partial T}{\partial x} + v\frac{\partial T}{\partial y} = \frac{1}{\left(\rho C_p\right)_{hnf}}\left(k_{hnf} + \frac{16\sigma^* T_\infty^3}{3k^*}\right)\frac{\partial^2 T}{\partial y^2}. \tag{6}$$

According to Zeyghami and Rahman [13], the dimensionless variables for model simplification are as follows:

$$\begin{gathered} u = \frac{2\nu_f}{x}Gr_x^{1/2} f'(\eta),\ v = -\frac{\nu_f}{x}\left(\frac{Gr_x}{4}\right)^{1/4}\left[3f(\eta) - \eta f'(\eta)\right], \\ \theta(\eta) = \frac{T - T_\infty}{\left(T_w - T_\infty\right)},\ \eta = \frac{y}{x}\left(\frac{1}{4}Gr_x\right)^{1/4}, \end{gathered} \tag{7}$$

also,

$$v_w = -\frac{3\nu_f}{x}\left(\frac{Gr_x}{4}\right)^{1/4} S, \tag{8}$$

where the prime notation signifies differentiation with respect to η, S is the constant mass flux velocity such that $S > 0$ is for suction and $S > 0$ is for injection, and $Gr_x = g\beta_f\left(T_w - T_\infty\right)x^3/\nu_f^2$ is the constant Grashof number based on the length $L = x$ of the plate.

Substituting the similarity variables (7) into Eqs. (2) and (6), one gets:

$$\frac{\mu_{hnf}/\mu_f}{\rho_{hnf}/\rho_f} f''' + 3ff'' - 2f'^2 + \frac{\beta_{hnf}}{\beta_f}\theta = 0, \tag{9}$$

$$\frac{1}{\Pr}\frac{1}{\left(\rho C_p\right)_{hnf}/\left(\rho C_p\right)_f}\left(\frac{k_{hnf}}{k_f} + \frac{4}{3}Rd\right)\theta'' + 3f\theta' = 0, \tag{10}$$

subject to the boundary conditions:

$$\begin{gathered} f(0) = S,\ f'(0) = 0,\ \theta(0) = 1, \\ f'(\eta) \to 0,\ \theta(\eta) \to 0 \text{ as } \eta \to \infty, \end{gathered} \tag{11}$$

where $\Pr = \nu_f\left(\rho C_p\right)_f / k_f$ is the Prandtl number, and $Rd = 4\sigma^* T_\infty^3 / k^* k_f$ is the radiation parameter.

The main quantities of physical are the skin friction C_{fx} and the local Nusselt number Nu_x,

$$C_{fx} = \frac{\mu_{hnf}}{\rho_f u_w^2}\left(\frac{\partial u}{\partial y}\right)_{y=0},\ Nu_x = -\frac{xk_{hnf}}{k_f\left(T_w - T_\infty\right)}\left(\frac{\partial T}{\partial y}\right)_{y=0} + \frac{x}{k_f\left(T_w - T_\infty\right)}\left(q_r\right)_{y=0}, \tag{12}$$

Using (7) and (12), one gets,

$$2\left(4Gr_x\right)^{1/4} C_{fx} = \frac{\mu_{hnf}}{\mu_f} f''(0),\ 2\left(4Gr_x\right)^{-1/4} Nu_x = -\left(\frac{k_{hnf}}{k_f} + \frac{4}{3}Rd\right)\theta'(0). \tag{13}$$

It should be mentioned here that for a regular fluid $\left(\phi_1 = \phi_2 = 0\right)$, Eq. (9) is similar with Eq. (16) from Zeyghami and Rahman [13].

3. Results and discussion

The mathematical model of Eqs. (9)-(11) has been successfully solved using bvp4c in Matlab. For validation purposes, we have compared our numerical outputs with the prior findings of $f''(0)$ and $-\theta'(0)$ (see Tab. 3), for the case when $\phi_1 = \phi_2 = S = Rd = 0$. This comparison shows a perfect agreement and thus validates our model and the numerical calculations in the solver. In this present numerical analysis, we consider the value of the Prandtl number to be 6.2, with constant 1% volume fraction of alumina, meanwhile, for the other parameters, the following allocation of the range are specified: $0\% \le \phi_2 \le 2\%$ (volume fraction of copper), $0 \le S \le 2$ (suction parameter), and $0 \le Rd \le 5$ (thermal radiation parameter). To analyze the impact of each control parameter, we have generated the graphical illustration of velocity $f'(\eta)$ and temperature $\theta(\eta)$ profiles (see Figs. 2-5), as well as the numerical outputs for the local skin friction coefficient $2(4Gr_x)^{1/4} C_{fx}$ and the local Nusselt number $2(4Gr_x)^{-1/4} Nu_x$ (see Tab. 4).

Table 3. Comparison value of the numerical outputs

Pr	$f''(0)$		$-\theta'(0)$	
	Present (bvp4c)	Ostrach [20]	Present (bvp4c)	Ostrach [20]
0.72	0.676019511	0.6760	0.504634169	0.5046
0.733	0.674181954	0.6741	0.507907671	0.5080
1	0.642188152	0.6421	0.56714600	0.5671
2	0.571263133	0.5713	0.716466728	0.7165
6.2	0.461834471		1.017250891	

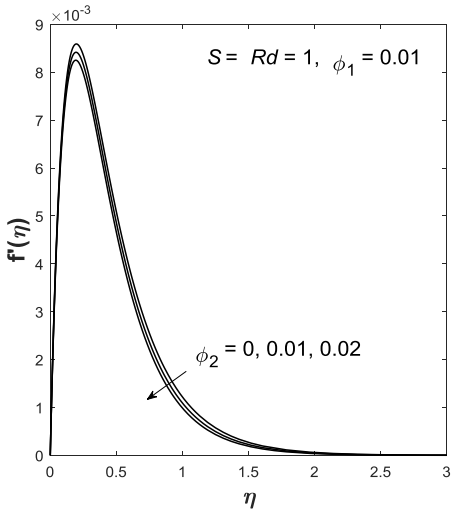

Figure 2. Velocity profile for copper volume fraction

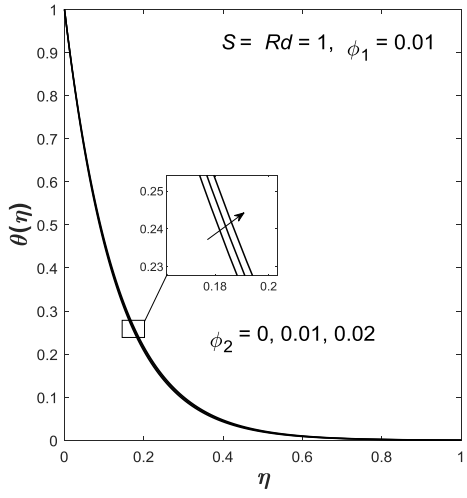

Figure 3. Temperature profile for varied copper volume fraction

The impact of ϕ_2 (the second nanoparticles) towards the velocity and the temperature of the fluid flow are shown in Figs. 2 and 3. Under the configurations when $Rd = S = 1$ and in the presence of natural convection, the increment of ϕ_2 from 0% to 2% has caused a decrement in the velocity profile, but oppositely, enlarging the temperature profile. The plot of the velocity profile (see Fig. 2) is seen to initially increase up to a certain point and then gradually decrease as $\eta \to \infty \approx 3$. The highest peak for the velocity profile is observed to be approximately at 8×10^{-3} which is for the case when

$\phi_2 = 2\%$. The thickness of the momentum boundary layer also is noticed to be reducing as ϕ_2 is increasing, but oppositely for the thermal boundary layer. A decreasing concave-up plot is illustrated for the temperature profile such that $\theta(\eta) \to 0$ as $\eta \to \infty$, which fulfills the condition for the far-field boundary.

Figures 4 and 5 depict the velocity and temperature profiles for several values of thermal radiation parameter. The velocity and temperature profiles are contemplated to amplify when we upgrade the Rd from 1 to 5. The same pattern in the relations between Rd and $\theta(\eta)$ is also shown by Jha and Samaila [21], though they did not consider the hybrid nanofluid. The momentum and thermal thicknesses of the boundary layer are also getting thicker as larger Rd is used. All these graphical findings of profiles produced the same pattern of plots as those by Ostrach [20] regardless of the variation of control parameters.

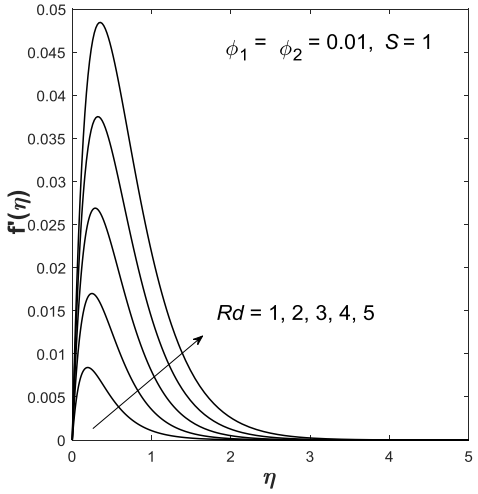

Figure 4. Velocity profile for varied thermal radiation

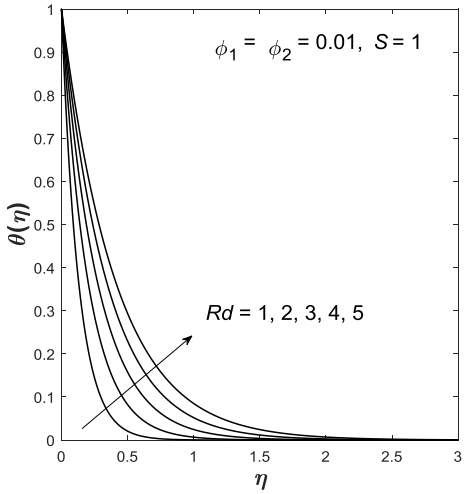

Figure 5. Temperature profile for varied thermal radiation

For the main physical quantities, we present the outputs in the form of numerical data as presentable in Tab. 4. According to our configurations, higher skin friction is achievable by enlarging ϕ_2 and Rd while reducing S. Meanwhile, to establish a higher heat transmission rate (local Nusselt number), it is suggestible to increase Rd and S, while lessening ϕ_2. These findings are based on the existence of natural or free convection. The heat transmission rate is seen to enlarge extensively when suction is imposed.

Table 4. Value of local skin friction coefficient and local Nusselt number

ϕ_2	S	Rd	$2(4Gr_x)^{1/4} C_{fx}$	$2(4Gr_x)^{-1/4} Nu_x$
0	0	1	0.544157531	1.829450424
0.01			0.546092011	1.826001876
0.02			0.548198634	1.822539641
0	1	1	0.125930532	18.562864481
0.01			0.127478667	18.530344937
0.02			0.129005740	18.497821585
0	1	0	0.054988736	18.550877528
0.01			0.056620319	18.518468963
0.02			0.058230974	18.486059249
0	1	2	0.195826809	18.592998943

0.01			0.197321786	18.559606412
0.02			0.198793711	18.526259206
0	2	1	0.063129377	37.100806565
0.01			0.063904747	37.035838136
0.02			0.064669528	36.970869235

4. Statistical analysis: Response surface methodology

Response surface methodology (RSM) is among the various experimental design methods that can be employed to enhance processes and systems. RSM encompasses a range of mathematical and statistical techniques that evaluate the response of a system to the input variables and create a mathematical model to predict its behavior. Through RSM, the ideal values for input variables can be determined and the performance of a system can be enhanced. In the present study, RSM can be utilized to identify the input variables (parameters) that have the most significant impact on heat transmission performance (response).

Therefore, for this analysis, the interactive effects between Rd, ϕ_1, and ϕ_2 towards heat transmission are explored. These three parameters are designated with three levels which are low, medium, and high (see Tab. 5). The experimental design for the parameters and response in 20 runs via the face-centered composite design is exemplified in Tab. 6, where the other parameters are put as constant such that $\mathrm{Pr} = 6.2$ and $S = 2$. To scrutinize the correlative impacts of the parameters on the heat transmission rate, the following general quadratic model is introduced:

$$response = \alpha_i A + \alpha_i B + \alpha_i C + \alpha_i AB + \alpha_i AC + \alpha_i BC + \alpha_i A^2 + \alpha_i B^2 + \alpha_i C^2 + \alpha_i , \quad (14)$$

where α_i $(i = 1, 2, ..., 10)$ are the acquired coefficients of the coded parameters.

Table 5. Parameters and levels

Parameters	Coded symbol	Levels		
		−1 (Low)	0 (Medium)	1 (High)
Rd	A	1	3	5
ϕ_1	B	0.01	0.015	0.02
ϕ_2	C	0.01	0.015	0.02

Table 6. Experimental design

Runs	Coded values			Real values			Responses
	A	B	C	Rd	ϕ_1	ϕ_2	Heat transmission rate
1	−1	−1	−1	1	0.01	0.01	37.035838136
2	1	−1	−1	5	0.01	0.01	37.068010894
3	−1	1	−1	1	0.02	0.01	36.934980487
4	1	1	−1	5	0.02	0.01	36.966444698
5	−1	−1	1	1	0.01	0.02	36.970869235
6	1	−1	1	5	0.01	0.02	37.001688751
7	−1	1	1	1	0.02	0.02	36.870012450
8	1	1	1	5	0.02	0.02	36.900182049
9	−1	0	0	1	0.015	0.015	36.952924933
10	1	0	0	5	0.015	0.015	36.984063322
11	0	−1	0	3	0.01	0.015	37.013383891
12	0	1	0	3	0.02	0.015	36.912350140
13	0	0	−1	3	0.015	0.01	36.995527077
14	0	0	1	3	0.015	0.02	36.930212843
15	0	0	0	3	0.015	0.015	36.962866352

16	0	0	0	3	0.015	0.015	36.962866352
17	0	0	0	3	0.015	0.015	36.962866352
18	0	0	0	3	0.015	0.015	36.962866352
19	0	0	0	3	0.015	0.015	36.962866352
20	0	0	0	3	0.015	0.015	36.962866352

Further, with the aid of Minitab software, we generate the regression model, and the data analysis for the model is carried out through the analysis of variance (ANOVA) as tabulated in Tab. 7. If the p-value of a parameter is less than 0.05, it is regarded as statistically significant, indicating a 95% level of significance. Hence, in this case, from Tab. 7, it is noticed that the variables of B^2, C^2, and BC are not significant in the designated model and need to be omitted. Therefore, to fit the model, we have omitted the non-significant variables, rerun the analysis, and refitted the model. Consequently, the finalized regression model for response (heat transmission rate) is as follows:

$$response = 0.015576A - 0.050582B - 0.032784C - 0.00017AB - 0.000331AC + 0.005634A^2 + 36.9629. \quad (15)$$

Table 7. Analysis of variance (1st run)

Source	Degree of freedom	Adjusted sum of squares	Adjusted mean squares	F-value	p-value
Model	9	0.038919	0.004324	844556.36	0.000
Linear	3	0.038759	0.012920	2523263.78	0.000
A	1	0.002426	0.002426	473853.10	0.000
B	1	0.025585	0.025585	4996901.22	0.000
C	1	0.010748	0.010748	2099037.02	0.000
Square	3	0.000159	0.000053	10333.19	0.000
*A*A*	1	0.000087	0.000087	17021.20	0.000
*B*B*	1	0.000000	0.000000	0.00	(0.956)
*C*C*	1	0.000000	0.000000	0.02	(0.903)
Interaction	3	0.000001	0.000000	72.10	0.000
*A*B*	1	0.000000	0.000000	45.05	0.000
*A*C*	1	0.000001	0.000001	171.16	0.000
*B*C*	1	0.000000	0.000000	0.09	(0.772)
Error	10	0.000000	0.000000		
Lack-of-fit	5	0.000000	0.000000	*	*
Pure error	5	0.000000	0.000000		
Total	19	0.038919			

Note: ( ) indicates the non-significant p-value

Table 8. Analysis of variance for the fitted regression model (2nd run)

Source	Degree of freedom	Adjusted sum of squares	Adjusted mean squares	F-value	p-value
Model	6	0.038919	0.006487	1627807.48	0.000
Linear	3	0.038759	0.012920	3242244.84	0.000
A	1	0.002426	0.002426	608873.23	0.000
B	1	0.025585	0.025585	6420722.75	0.000
C	1	0.010748	0.010748	2697138.52	0.000
Square	1	0.000159	0.000159	39832.57	0.000
*A*A*	1	0.000159	0.000159	39832.57	0.000
Interaction	2	0.000001	0.000001	138.91	0.000
*A*B*	1	0.000000	0.000000	57.89	0.000
*A*C*	1	0.000001	0.000001	219.93	0.000

Error	13	0.000000	0.000000		
Lack-of-Fit	8	0.000000	0.000000	*	*
Pure Error	5	0.000000	0.000000		
Total	19	0.038919			

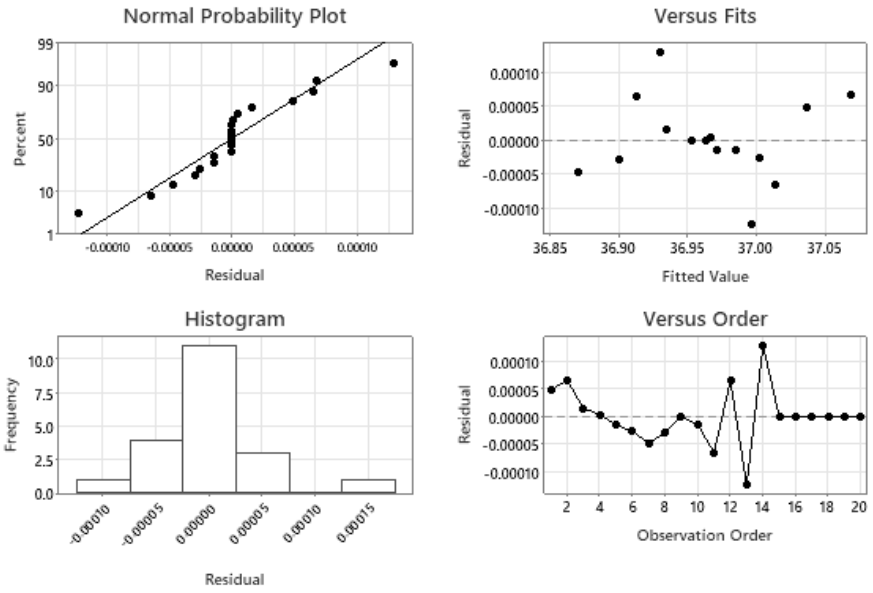

Figure 6. Residual plots for response

The ANOVA tabulation for this finalized regression model is displayed in Tab. 8, showing that all variables are now statistically significant. A 100% R-squared is attained which signifies that the model explains all the variability of the response around its mean with a standard error of regression 0.0000631. Besides, the accuracy of the model can be determined through the residual plots shown in Fig. 6. The alignment of data points along a straight line in the normal probability plot and the bell-shaped histogram suggest that the residuals follow a normal distribution. Additionally, the correctness of the model is implied by the maximum error of the estimated values being 0.00015, confirming it as a good fit. The model in Eq. (15) shows that the response (heat transmission rate) is negatively affected by the coefficients of *B, C, AB,* and *AC*. The analysis of the interactive effect of the (coded) parameters on the heat transmission rate (response) can be contemplated through the surface and contour plots as displayed in Fig. 7. The interpretation of Fig. 7 can be listed respectively as follows:

1. The maximum response can be established with a high-level of *A* and low-level of *B*, while holding *C* in the medium-level.
2. The maximum response can be established with a high-level of *A* and low-level of *C*, while holding *B* in the medium-level.
3. The maximum response can be established with a low-level of *B* and low-level of *C*, while holding *A* in the medium-level.

This given interpretation can be examined and verified in greater detail by applying the optimization technique. To achieve this, the following desirability function is given:

$$D = \prod_{i=1}^{n} \left(d_i^{r_i} \right)^{\frac{1}{\sum r_i}}, \tag{16}$$

where r_i is the importance value for n responses and d_i is the desirability. Since the maximization of heat transmission rate becomes the main concern, thence, the maximization desirability is expressed as:

$$d_i = \frac{R_i - R_{L,i}}{R_{H,i} - R_{L,i}}, \tag{17}$$

where R_i, $R_{L,i}$, and $R_{H,i}$ are the predicted response, lowest response, and highest response, respectively. Therefore, with the facilitation of built-in optimizer in Minitab, the maximum heat transmission rate is approximated to be 37.0679 when $Rd = 5\,(A = 1)$, $\phi_1 = 1\%$ $(B = -1)$ and $\phi_2 = 1\%$ $(C = -1)$. These optimization values for the control parameters in achieving the maximum response (heat transmission rate) is also evident through the contour plot in Fig. 7. The coded parameter *A* has a dominant effect towards the response among all the parameter combinations.

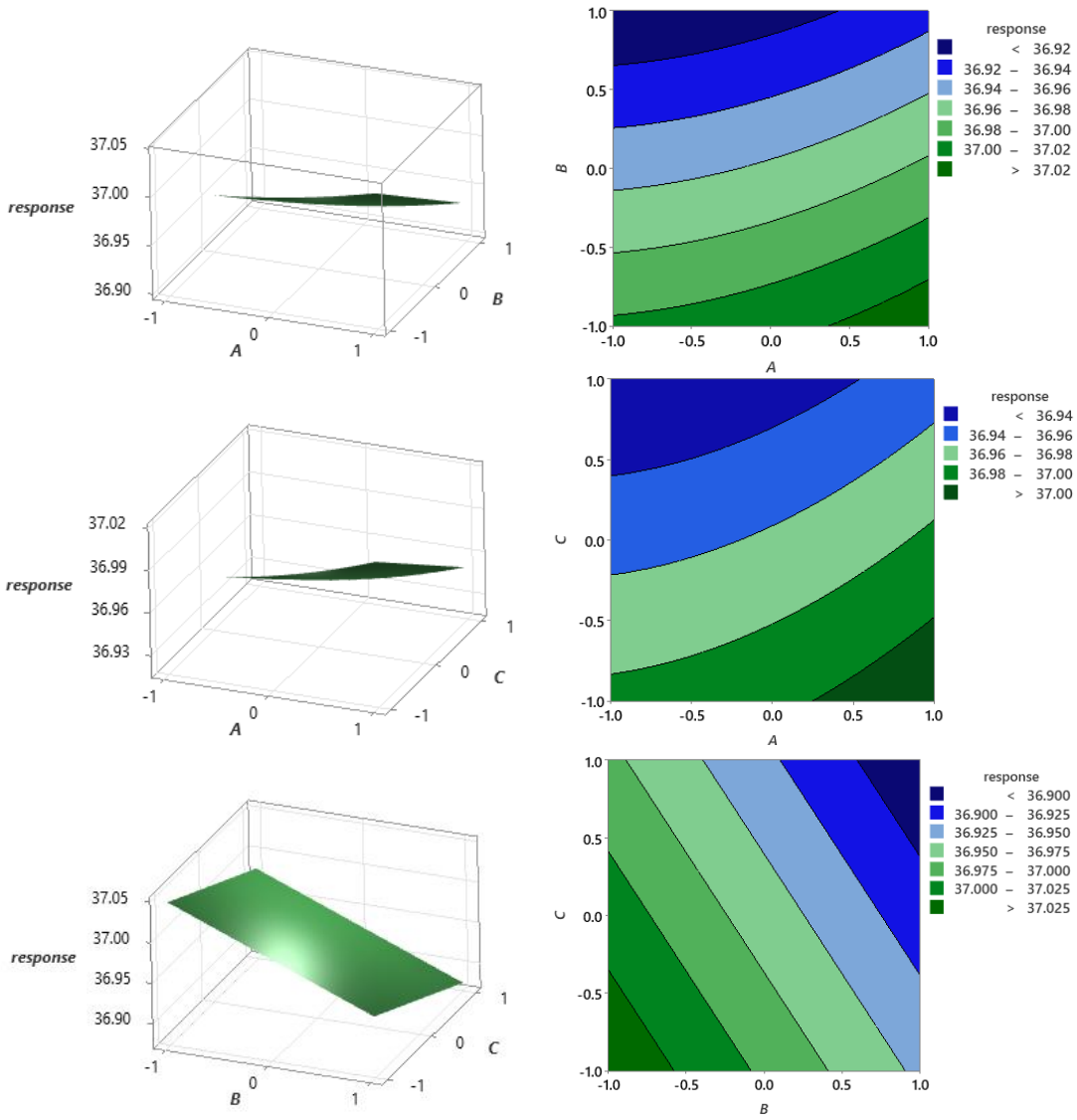

Figure 7. Surface and contour plots of response for different combinations of parameter

5. Conclusion

The mathematical and statistical analyses towards the natural convection of a hybrid nanofluid on a vertical plate with radiation effect have been successfully elucidated. We have scrutinized the impacts of the considered control parameters towards the flow and the heat transmission of the hybrid nanofluid model together with their maximum desirability criteria. The following key points summarize the findings of this present study:

- The inclusion of copper and the upsurge in its volume fraction in the hybrid nanofluid suspension has reduced the velocity profile and the local Nusselt number but increased the temperature profile and the local skin friction.
- Higher suction strength causes the local skin friction to decrease but enhances the heat transmission rate (local Nusselt number).
- Stronger thermal radiation could be used to improve the fluid velocity and temperature as well as the heat transmission rate.
- Through the optimization via RSM, the maximum heat transmission rate is achievable by the usage of $Rd = 5$, $\phi_1 = 1\%$ and $\phi_2 = 1\%$ with the desirability of 99.97%.

It is important to acknowledge that the findings showcased in this study are constrained by the specific model and parameters that were utilized. Thus, to obtain a more thorough comprehension of the topic and to obtain practical insights that hold potential for numerous industrial applications, it is strongly advised to conduct additional investigations using varied parameters and nanofluid compositions.

Acknowledgment

The authors acknowledge the Ministry of Higher Education (MOHE) Malaysia and Universiti Putra Malaysia for the funding under the Fundamental Research Grant Scheme (FRGS) (FRGS/1/2023/STG06/UPM/02/1) and Vote no.: 5540632. The work by Ioan Pop has been supported by Grant PN-III-P4-PCE-2021-0993, UEFISCDI, Romania.

Nomenclature

A, B, C – coded symbols
C_{fx} – skin friction coefficient
C_p – specific heat capacity [$Jkg^{-1}K^{-1}$]
f – dimensionless stream function
Gr_x – Grashof number
k – thermal conductivity [$Wm^{-1}K^{-1}$]
k^* – mean absorption coefficient [m^{-1}]
L – characteristic length
Nu_x – Nusselt number
Pr – Prandtl number
q_r – radiative heat flux [Wm^{-2}]
Rd – thermal radiation parameter
S – suction/injection parameter
T – fluid temperature [K]
T_w – surface temperature [K]
T_∞ – ambient temperature [K]
u, v – velocity components [ms^{-1}]
v_w – mass flux velocity [ms^{-1}]
x, y – Cartesian coordinates [m]

Greek symbols
β – thermal expansion [K^{-1}]
η – dimensionless similarity variable
θ – dimensionless temperature function
ρ – density [kgm^{-3}]
σ^* – Stefan Boltzmann-constant [$Wm^{-2}K^{-4}$]
ϕ_1, ϕ_2 – volume fraction of nanoparticles

Subscripts
f – base fluid
hnf – hybrid nanofluid
$s1$ – first nanoparticles
$s2$ – second nanoparticles

Supercript
' – differentiation respect to η

References

[1] Choi, S.U.S., Eastman, J.A., Enhancing Thermal Conductivity Of Fluids With Nanoparticles, *ASME Fluids Eng. Div*, *231* (1995), pp. 99-106
[2] Babu, J.R., et al., State-Of-Art Review On Hybrid Nanofluids, *Renewable and Sustainable Energy Reviews*, *77* (2017), pp. 551-565
[3] Sarkar, J., et al., A Review On Hybrid Nanofluids: Recent Research, Development And Applications, *Renewable and Sustainable Energy Reviews*, *43* (2015), pp. 164-177
[4] Suresh, S., et al., Synthesis Of Al_2O_3–Cu/Water Hybrid Nanofluids Using Two Step Method And Its Thermo Physical Properties, *Colloids and Surfaces A: Physicochemical and Engineering Aspects*, *388* (2011), 1-3, pp. 41-48
[5] Suresh, S., et al., Effect Of Al_2O_3–Cu/Water Hybrid Nanofluid In Heat Transfer, *Experimental Thermal and Fluid Science*, *38* (2012), pp. 54-60
[6] Devi, S.P.A., Devi, S.S.U., Numerical Investigation Of Hydromagnetic Hybrid Cu –Al_2O_3/Water Nanofluid Flow Over A Permeable Stretching Sheet With Suction, *International Journal of Nonlinear Sciences and Numerical Simulation*, *17* (2016), 5, pp. 249-257
[7] Devi, S.S.U., Devi, S.P.A., Numerical Investigation Of Three-Dimensional Hybrid Cu–Al_2O_3 /Water Nanofluid Flow Over A Stretching Sheet With Effecting Lorentz Force Subject To Newtonian Heating, *Can. J. Phys.*, *94* (2016), 5, pp. 490-496
[8] Wahid, N.S., et al., MHD Hybrid Nanofluid Flow With Convective Heat Transfer Over A Permeable Stretching/Shrinking Surface With Radiation, *HFF*, *32* (2022), 5, pp. 1706-1727
[9] Mohd, R., et al., The Thermal Properties Of Water-Based Hybrid Nanofluid (Cu-Al_2O_3) Beyond An Inclined Plane, *Therm sci*, *26* (2022), 6 Part A, pp. 4561-4570
[10] Khashi'ie, N.S., et al., Non-Axisymmetric Homann Stagnation Point Flow And Heat Transfer Past A Stretching/Shrinking Sheet Using Hybrid Nanofluid, *HFF*, *30* (2020), 10, pp. 4583-4606
[11] Yahaya, R.I., et al., Oblique Stagnation-Point Flow Past A Shrinking Surface In A Cu-Al_2O_3/H_2O Hybrid Nanofluid, *JSM*, *50* (2021), 10, pp. 3139-3152
[12] Algehyne, E.A., et al., Analysis Of The MHD Partially Ionized GO-Ag/Water And GO-Ag/Kerosene Oil Hybrid Nanofluids Flow Over A Stretching Surface With Cattaneo–Christov

Double Diffusion Model: A Comparative Study, *International Communications in Heat and Mass Transfer, 136* (2022), pp. 106205
[13] Zeyghami, M., Rahman, M.M., Analysis Of Combined Natural Convection And Radiation Heat Transfer Using A Similarity Solution, *Energy Research Journal*, *6* (2015), 2, pp. 64-73
[14] Takabi, B., Salehi, S., Augmentation Of The Heat Transfer Performance Of A Sinusoidal Corrugated Enclosure By Employing Hybrid Nanofluid, *Advances in Mechanical Engineering*, *6* (2015), pp. 147059
[15] Oztop, H.F., Abu-Nada, E., Numerical Study Of Natural Convection In Partially Heated Rectangular Enclosures Filled With Nanofluids, *International Journal of Heat and Fluid Flow, 29* (2008), 5, pp. 1326-1336
[16] Devi, S.U., Devi, S.A., Heat Transfer Enhancement Of Cu-Al_2O_3/Water Hybrid Nanofluid Flow Over A Stretching Sheet, *Journal of the Nigerian Mathematical Society, 36* (2017), 2, pp. 419-433
[17] Rosseland, S., *Astrophysik Auf Atomtheoretischer Grundlage*, J. Springer, Berlin, 1931
[18] Cortell Bataller, R., Radiation Effects In The Blasius Flow, *Applied Mathematics and Computation*, *198* (2008), 1, pp. 333-338
[19] Ishak, A., et al., Radiation Effects On The Thermal Boundary Layer Flow Over A Moving Plate With Convective Boundary Condition, *Meccanica*, *46* (2011), 4, pp. 795-801
[20] Ostrach, S., An Analysis Of Laminar Free-Convection Flow And Heat Transfer About A Flat Plate Parallel To The Direction Of The Generating Body Force, *NACA, TN 2635*, (1952), pp. 50
[21] Jha, B.K., Samaila, G., A Similarity Solution For Natural Convection Flow Near A Vertical Plate With Thermal Radiation, *Microgravity Sci. Technol., 32* (2020), 6, pp. 1031-1038

Submitted: 12.11.2023.
Revised: 28.04.2024
Accepted: 26.05.2024